Yunbo Li
Zongyu Tang
Jiaye Gong

http://dx.doi.org/10.21278/brod74408

ISSN 0007-215X
eISSN 1845-5859

The effect of PID control scheme on the course-keeping of ship in oblique stern waves

UDC 629.5.022.3:629.5.017.3:681.515.8
Original scientific paper

Summary

Sailing in oblique stern waves causes a ship to make sharp turns and uncontrollable course deviation, which is accompanied by a large heel and sometimes leads to capsizing. Studying the control algorithm in oblique stern waves is imperative because an excellent controller scheme can improve the ship's course-keeping stability. This paper uses the Maneuvering Modelling Group (MMG) method based on hydrodynamic derivatives and the Computational Fluid Dynamics (CFD)-based self-navigation simulation to simulate ship navigation in waves. This study examines the effect of proportion-integral-derivative (PID) controller schemes on the stability of course maintenance based on hydrodynamic derivatives and 3DOF MMG methods. Then, the optimized PID control parameters are used to simulate the ship's 6DOF self-propulsion navigation in oblique waves using the CFD method. The nonlinear phenomena during the process, such as side-hull emergency, slamming, and green water, are considered. This study found that the range of the control bandwidth should be optimized based on the ship's heading and wave parameters.

Keywords: *Trimaran; oblique stern wave; PID scheme; CFD method; manoeuvrability*

1 Introduction

In general, waves significantly affect a ship's motion characteristics and are the key factors affecting course-keeping, which has been widely studied in recent years [1-3]. Among them, stern and oblique waves have the most severe impact on ship navigation safety [4-5], making the ship lose control. At the 22nd ITTC conference, more than 20 institutions from 13 countries worked together to investigate the causes of ship capsizing. Statistics show that 65% of ships sailing in oblique stern waves experienced significant course deviation and loss of steering control. This process is accompanied by a large heeling, which may eventually lead to capsizing. In the Second Generation Intact Stability Criteria by the International Maritime Organization, surf-riding/broaching is listed as one of five stability failure modes [6]. In addition, oblique stern waves usually cause surf riding/broaching. An optimal steering control strategy can reduce the roll angle [7-8]. Therefore, studying the control algorithm in the oblique stern waves is significant.

The PID controller is widely used in various industries. Minorsky et al. [9] were the first to study the PID control for ship course-keeping. They applied different automatic controller schemes to control the ship's course. Van et al. [10] deduced the range of the natural oscillation frequency using the first-order Nomoto model, and this frequency (ω_n) has a significant impact on the PID parameters. Additionally, Namkyun et al. [11] demonstrated PD's effectiveness in maintaining the stability of vessel course-keeping by successfully implementing a proportional-derivative (PD) control scheme for heading regulation during the ship's turning circle manoeuvre.

Hashimoto et al. [12] calculated the PD parameters for simulating ships' autopilot in waves based on the hydrodynamic derivatives. They used mean wave force and moment to simulate ship motion while employing the PD-based autopilot. Fossen et al. [7] proposed optimizing the damping coefficient and control bandwidth to enhance heading control according to working conditions. They also proposed a calculation method for the natural oscillation frequency. Jong et al. [5] used the PD controller and self-propulsion simulation method to predict the surf-riding and broaching of ships. Although novel and sophisticated control methodologies are available, the conventional PID controller remains widely used due to its simplicity and practical implementation advantages [13]. Umeda et al. [14] employed a PD controller to control the rudder angle in numerical simulation of ship motion in waves. Sadat-Hosseini et al. [15] discussed manoeuvring in calm water and regular waves for surface combatants (ONR tumblehome and 5415M). The study compared roll-induced and drift-induced hydrodynamic forces between CFD and Experimental Fluid Dynamics (EFD). The results showed that the Reynolds-averaged Navier-Stokes (RANS) solver of CFD Ship-Iowa can estimate roll-induced and drift-induced hydrodynamic forces with reasonably accurate results [16, 17].

From the viewpoint of the control scheme, the optimal control scheme is effective for improving the course-keeping performance in oblique stern waves. The ship heading automatic control system, usually based on PID control, is currently the most widely used system [18]. The research on ship course-keeping in waves began in the 1920s, and classical control theory is applied to ship course-keeping. Dubey et al. [19] applied the classical PID control and 3DOF MMG to simulate the navigation of the KVLLC2 model in calm water and waves. They compared the experimental results with the numerical model results. Numerical and self-propelled simulations are usually related to course-keeping control in stern waves, where the rudder angle is controlled by a proportional-derivative (PD) controller [20]. The above literature shows that despite new developments in ship control, the PD controller method is still widely used to control ship heading in stern waves [5, 8, 19].

Fossen et al. [7] proposed optimizing the PID controller by modifying the damping factors and control bandwidth to optimize the parameters of the PID controller. Maki et al. [8] pointed out that steering at a small Froude Number could help ships avoid course deviation caused by stern waves. Maniyappan et al. [21] demonstrated that the disappearance of rudder force is one of the main reasons for capsizing in oblique stern waves. Still, an optimal PD control scheme can effectively prevent ship capsizing. It is evident that when using PID control for ship course-keeping, the corresponding control parameters need to be optimized based on the working conditions. The value of the natural oscillation frequency significantly influences the PID controller’s performance [7].

The 3DOF MMG method based on the hydrodynamic derivatives and the CFD-based 6-DOF simulation is still widely used to simulate the ship's autopilot in waves. The control of 6DOF is often deemed too complex for most ships. Hence, ship dynamics are commonly represented by the 3DOF manoeuvring model, such as the MMG model [7]. Yasukawa et al. [24] utilized the 3DOF ship model of the KVLCC2 tanker and employed the hydrodynamic

derivative-based MMG method to investigate the simulation of turning manoeuvres in calm and regular waves. Castiglione et al. [22] conducted CFD simulations to examine the seakeeping performance of a catamaran model under both head and oblique regular waves at two Froude numbers. In two cases, Carrica et al. [23] used the ship hydrodynamics code CFDShip-Iowa v4.5 to simulate broaching in regular waves. The study employed a PID control algorithm to effectively reduce the rolling moment of the ship, thereby enhancing its steering performance.

Yasukawa et al. [25] used the 4DOF MMG equation of surge-sway-bow-roll to describe the ship's motion and numerically simulated the ship's motion under the influence of wind and waves. Hosseini et al. [26] assessed the 6DOF CFD method to simulate the ship motion with different initial wave headings and compare the errors of the CFD and potential flow (PF) methods. Kim et al. [27] simulated the course-keeping of the KCS container ship in waves and the turning motion in head waves using the CFD-based technique and investigated the effect of wavelength on ship manoeuvrability. Gong et al. [28-29] applied the CFD method to simulate an autonomous trimaran in a stern wave and studied the effect of muzzle velocity on the sailing of a trimaran model in stern waves.

Due to the wide range of control parameters in the studies of ship course control, the MMG method based on hydrodynamic derivative regression with higher computational efficiency is mainly used. Still, the nonlinear effects such as large-scale ship motion and water in and out are ignored [30-31]. Self-propulsion simulations can better reflect the ship sailing process in waves, but the MMG approach is more efficient for large-scale studies.

This paper studies the influence of the PID control strategy on trimaran's navigation in waves. Taking advantage of the MMG method's high efficiency, the 3DOF MMG method was used to initially simulate the motion of a trimaran in still water and waves. The calculated results are compared with the experimental values for validation. The 3DOF MMG method was used to pre-study the effect of PID parameters on the course-keeping of the trimaran in the waves, and three PID parameters were selected. Then, a hybrid method was used to simulate the 6DOF autopilot of the trimaran in waves with the three PID parameters. The hybrid method is based on the fully nonlinear potential theory and the viscous flow method [32-33]. The course-keeping performance of a trimaran with different natural frequencies and PID parameters in waves was studied by analysing the computed results.

2 Numerical Approaches

This section introduces the principle of the 3DOF MMG method, 6DOF autopilot simulation, and the selection of the PID parameter.

2.1 Basic Equations of Numerical Simulation

This study uses the local coordinate system *o*'-*x*'*y*'*z*' to solve the trimaran's motion. The origin of the local coordinate system is located at the trimaran's centre of gravity. The *x*'-axis points to the bow, and the *y*'-axis points to the port side. The 3DOF MMG equations used to calculate the autopilot of the trimaran in the stern wave are given below.

$$(m+m_x)\dot{u}-(m+\mathrm{m}_y)vr=X_H+X_{wj}+X_w \tag{1}$$

$$(m+m_x)\dot{u}-(m+m_y)vr=X_H+X_{wj}+X_w \tag{2}$$

$$(I_{zz}+J_{zz})\dot{r}=N_H+N_{wj}-Y_H\cdot x_G+N_w \tag{3}$$

where the variables are in the ship-fixed coordinate system, m is the mass of the trimaran, (m_x, m_y) are the ship's longitudinal, transverse components of the mass, (u, v, r) and ($r_{z'}$) are the linear and angular velocity, respectively. (I_{zz}, J_{zz}) is the inertia moment. (H, wj, and W) are bare hull, waterjet, and wave, respectively [34].

At the beginning of the simulation, the gross thrust of the water jet is equal to the resistance in the calm water. Then, when the nozzle is deflected to control the heading of the trimaran, the thrust and steering force of the water jet are obtained by the conservation of momentum to the thrust deflection [5]. The same water jet model is used for both MMG and CFD simulations. The wave force and moment are obtained from the second-order average wave force, and these wave force simulation methods are also presented in [[1], [33]].

Hydrodynamic forces acting on the ship hull are expressed as follows.

$$X_H = -R_0 + X_{vv}v^2 + X_{vr}vr + X_{rr}r^2 \tag{4}$$

$$Y_H = Y_v v + Y_r r + Y_{vvv}v^3 + Y_{vvr}v^2 r + Y_{vrr}vr^2 + Y_{rrr}r^3 \tag{5}$$

$$N_H = N_v v + N_r r + N_{vvv}v^3 + N_{vvr}v^2 r + N_{vrr}vr^2 + N_{rrr}r^3 \tag{6}$$

where the hydrodynamic derivatives X_{vv}, X_{vr}, X_{rr}, Y_v, Y_r, Y_{vvv}. , Y_{vvr}, Y_{vrr}, Y_{rrr}, N_v, N_r, N_{vvv}, N_{vvr}, N_{vrr}, N_{rrr} are determined by the captive model test. R_0 is the longitudinal viscous hydrodynamic factor [25], which represents the relationship between ship resistance and speed.

This study uses the semi-empirical model of the water jet thrust and steering moment [5, 28]. The water jet force values are based on the resistance of the bare hull without the water jet. At the beginning of the simulation, the trimaran heading was maintained by nozzle rotation. The total thrust of the water jet is equal to the resistance in still water. Adjust the nozzle deflection angle δ according to the yaw angle ξ and the yaw rate $\dot{\xi}$ to maintain the initial heading. The definitions of waterjet force and momentum X_{wj}, Y_{wj}, N_{wj} are as follows.

$$X_{wj} = (X_0 + X_u v_0 + X_{uu}{v_0}^2 + X_{uuu}{v_0}^3)\cos(DA) \tag{7}$$

$$Y_{wj} = -(X_0 + X_u v_0 + X_{uu}{v_0}^2 + X_{uuu}{v_0}^3)\sin(DA) \tag{8}$$

$$N_{wj} = (X_0 + X_u v_0 + X_{uu}{v_0}^2 + X_{uuu}{v_0}^3)\sin(DA)L \tag{9}$$

where v_0 is the initial ship speed, DA is the drift angle, L is the ship length, X_0 is the longitudinal viscous hydrodynamic factor [25], representing the relationship between ship resistance and speed, X_u, X_{uu}, X_{uuu}, are the hydrodynamic derivatives for the ship resistance.

The second-order average wave force acting on the ship is selected as follows. Daidolal [35] considered the influence of waves on ship manoeuvrability and proposed the following calculation formulas for wave drift force and wave moment.

$$X_{wave} = \alpha\rho g L\zeta_D^2 C_{XD}(\lambda)\cos(\chi) \tag{10}$$

$$Y_{wave} = \alpha\rho g L\zeta_D^2 C_{YD}(\lambda)\sin(\chi) \tag{11}$$

$$N_{wave} = \alpha\rho g L\zeta_D^2 C_{ND}(\lambda)\sin(\chi) \tag{12}$$

where ζ_D is the average wave amplitude, λ is the wavelength, and χ is the wave heading. Fig. 1 shows the definition of the wave heading. C_{XD} and C_{YD} are the wave drift force coefficients to the *x*' and *y*' directions, and C_{ND} is the wave drift moment coefficients around the *z*'-axis, α is the empirical correction factor, which is 0.5. The wave drift force and moment coefficients are as follows [36].

$$C_{XD} = 0.05 - 0.2(\frac{\lambda}{L}) + 0.75(\frac{\lambda}{L})^2 - 0.51(\frac{\lambda}{L})^3 \tag{13}$$

$$C_{YD} = 0.46 - 6.83(\frac{\lambda}{L}) - 15.65(\frac{\lambda}{L})^2 + 8.44(\frac{\lambda}{L})^3 \tag{14}$$

$$C_{ND} = -0.11 + 0.68(\frac{\lambda}{L}) - 0.79(\frac{\lambda}{L})^2 + 0.21(\frac{\lambda}{L})^3 \tag{15}$$

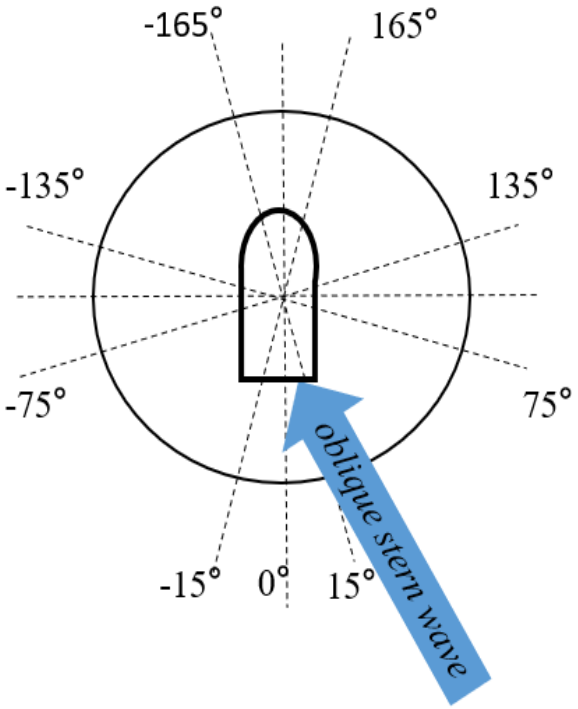

Fig. 1 Definition of wave direction

Local coordinate and global coordinate systems were used to simulate the ship's 6DOF autopilot in the wave. The local coordinate system is a ship-fixed coordinate system moving together with the ship. The Navier-Stokes equations are solved in the global coordinate system. The force and moment are transformed into the ship-fixed coordinate system to solve the ship's 6DOF motion [37]. In this paper, the trimaran's 6DOF autopilot in the stern waves was simulated using a hybrid method, which has been presented and used to study the nonlinear waves, seakeeping performance, and manoeuvrability of ships in our previous work [28, 29, 32, 38,39]. Hence, Section 4.2 gives a brief description of this method for completeness. QaleFOAM combines the potential-flow-based external wave tank [38-39] and the viscous-flow-based internal domain to simulate the motion of high-speed trimaran in regular wave with various wave directions to take advantage of potential flow theory and CFD method in wave simulation and motion simulation of trimaran [40].

During the simulation, the external domain is solved first in every time step: a one-phase flow. All boundaries of the internal domain are set as the interface, and the free surface elevation on the interface could be obtained using the external domain. Then, the external domain assigned the physical values on the internal domain interface. Note that the internal domain is a two-phase flow with no wind, so the velocity above water is set to zero on the interface. The trimaran is sailing freely, and the motions of the surge, sway, heave, roll, pitch, and yaw are considered using the hybrid method. The equations for solving the trimaran's motion are as follows [37]:

$$m(\dot{u}_x - v_y r_z + w_z r_y) = F_{Hx} + F_{WJx} \tag{16}$$

$$m(\dot{v}_y - w_z r_x + u_x r_z) = F_{Hy} + F_{WJy} \tag{17}$$

$$m(\dot{w}_y - u_x r_y + v_y r_x) = F_{Hz} + F_{WJz} \tag{18}$$

$$I_x r_x + (I_z - I_y) r_y r_z = M_{Hx} + M_{WJx} \tag{19}$$

$$I_y r_y + (I_x - I_x) r_x r_u = M_{Hx} + M_{WJz} \tag{20}$$

$$I_z r_z + (I_y - I_x) r_x r_y = M_{Hz} + M_{WJz} \tag{21}$$

where ($I_{x'}$, $I_{y'}$, $I_{z'}$) is the inertia moment, ($r_{y'}$, $r_{x'}$, $r_{z'}$) is the angular velocity, ($F_{Hx'}$, $F_{Hy'}$, $F_{Hz'}$) and ($M_{Hx'}$, $M_{Hy'}$, $M_{Hz'}$) are the hydrodynamic force and moment obtained by the viscous flow method. ($F_{WJx'}$, $F_{WJy'}$, $F_{WJz'}$) and ($M_{WJx'}$, $M_{WJy'}$, $M_{WJz'}$) are the force and moment of the water jet impetus. Since the results by the hybrid method do not distinguish between hydrostatic force and wave force, the wave force and moment at each time step are included in F_H and M_H. The simulation of the turn and zigzag manoeuvre by the current method was verified [32, 41].

Table 1 Boundary conditions of the computational domain

Boundary	Physical quantity			
	U	*alpha*	p_d	*k* / *omega* / *nut*
front/left/right	interface	interface	fixedFluxPressure	fixedValue
back	interface	interface	fixedFluxPressure	inletOutlet
top	pressureInletOutle	inletOutlet	totalPressure	inletOutlet
bottom	symmetryPlane	symmetry	symmetry	symmetry
hull surface	movingWall	zeroGradient	fixedFluxPressure	wallFunction

The turbulence model in this work is the SST k - ω model, which can simulate complex flow problems with flow separation and strong adverse pressure gradients. The two-phase flow in the internal domain is solved using the volume of fluid (VOF) method in the internal domain. It also models and predicts the distribution and movement of the immiscible phases interface [32]. An artificial compression technique [42-43] was used in OpenFOAM to keep the value consecutive and maintain a non-zero value only at the interface between air and water. Table 1 shows the boundary conditions applied to each boundary and dimension. During the 6DOF autopilot simulation, the roll, heave, and pitch motion are obtained from the dynamic

deformation mesh, horizontal movement, and yaw of the ship, simulated using the dynamic fluid body interaction (DFBI), which is realized by the motion of the internal domain. More details about the solution to the ship's motion can be found in [37]. Validation was performed using the KVLCC2 model [44], confirming the accuracy of wave frequency and pitch-roll frequency encountered by the vessel during autonomous navigation manoeuvres in wave conditions.

2.2 The PID Control Scheme

The PID control method is used to control the ship's course in this study. The effect of the controller scheme parameters on the course-keeping of a trimaran in oblique stern waves is discussed. The control algorithm for the nozzle angles is as follows:

$$\delta = K_p\xi + K_d\dot{\xi} + K_i\int_0^t \xi dt + K_m\dot{r} \tag{22}$$

where the initial heading 0◦, and 20◦ are the target, K_p is the proportional coefficient, K_d is the damping coefficient, K_i is the integral coefficient, K_m is the acceleration feedback gain, whose value is positive and generally small to prevent significant overshoot. $\dot{r}$ is the angular acceleration of the ship. The max nozzle angle and the changing rate of the nozzle are δ_{max} =25°and $\dot{\delta}$ =10°/s, respectively.

The PID control system could obtain the nozzle angle by inputting the error between the actual heading and the desired target heading in every time step to realize the autopilot. The control bandwidth can be determined by specifying the value of ω_n. Further details can be found in [6].

$$\omega_n = \frac{1}{\sqrt{1-2\zeta^2+\sqrt{4\zeta^4-4\zeta^2+2}}}\omega_b \tag{23}$$

The relative damping ratio ζ is usually chosen from 0.8 to 1.0. This study used ζ=1.0 [6], meaning that the control bandwidth ω_b is the only variable used to change the PID control parameters. Using the efficiency of the MMG method, ω_n for the oblique stern wave condition was selected by trial and error. Section 4.1 examines the choice of ω_n. According to different working conditions, it is necessary to specify the bandwidth ω_b (>0) and the relative damping ratio ζ (>0) to achieve the best control effect [12]. The gains of the PID feedback controller can be determined using pole placement based on the natural frequency. ω_n and the relative damping ratio ζ, resulting in

$$K_p = \frac{T+KK_m}{K}\omega_n, K_d = \frac{T+KK_m}{K}2\zeta\omega_n - \frac{1}{K}, K_i = \frac{T+KK_m}{10K}\omega_n^{\,3} \tag{24}$$

where *T* and *K* are ship manoeuvrability coefficients calculated using the hydrodynamic derivatives, obtained through tank tests. The calculation method for parameters *T* and *K* are as follows.

$$K = \frac{Y_\delta N_v + N_\delta Y_v}{Y_\delta N_r + N_v(mu_1 - Y_r)} \tag{25}$$

$$T = T_1 + T_2 - T_3 \tag{26}$$

$$T_1 + T_2 = \frac{-N_r(m - Y_{\dot{v}}) - (I_{zz} - N_{\dot{r}})Y_v - Y_{\dot{r}}N_v + (mu_1 - Y_r)N_{\dot{v}}}{Y_v N_r + N_v(mu_1 - Y_v)} \tag{27}$$

$$T_3 = \frac{Y_\delta N_{\dot{v}} + N_\delta(m - Y_{\dot{v}})}{Y_\delta N_r - N_\delta Y_v} \tag{28}$$

where $Y_{\dot{v}}$, $Y_{\dot{r}}$, $N_{\dot{r}}$, and $N_{\dot{v}}$ are the acceleration derivatives. Y_δ and N_δ are the hydrodynamic derivatives of the nozzle angle. Table 2 shows the trimaran's hydrodynamic coefficient. K_m can be specified as a percentage of the total moment of inertia:

$$K_m = \frac{\alpha}{100} m \tag{29}$$

where $\alpha \in [0,100]$. Since this study does not consider the influence of acceleration on heading control, α is set to 0.

Table 2 Hydrodynamic derivatives of trimarans

X_{vv}	X_{vr}	X_{rr}	Y_v	Y_r	Y_{vvv}	Y'_{vvr}	Y_{vrr}
-9.80	-13.86	-3.65	-186.29	-82.33	-259.95	-355.24	-580.56
Y_{rrr}	N_v	N_r	N_{vvv}	N_{vvr}	N_{vrr}	N_{rrr}	Y_δ
-564.06	-286.63	-229.44	-261.37	-1251.10	-1001.62	-2671.85	-17.76
N_δ	$Y_{\dot{v}}$	$Y_{\dot{r}}$	$N_{\dot{v}}$	$N_{\dot{r}}$			
35.53	29.56	-83.87	24.17	564.42			

3 Validation and Verification

The 6DOF CFD method has been widely applied in wave generation [32], ship's motion in waves [41], [45], and manoeuvring simulation of ships [44]. The corresponding validation has been carried out in our previous work. Hence, this section only compares the computed results using the 3DOF MMG method with the experimental results for validation before the study.

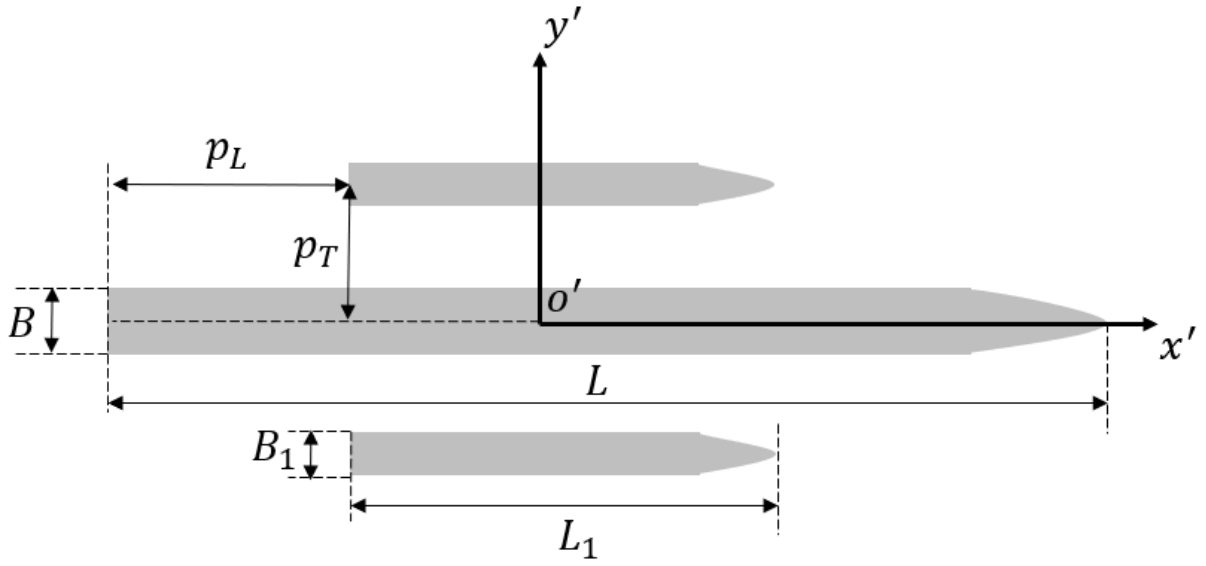

Fig. 2 Sketch and main characteristic dimensions of the trimaran

The trimaran model used in this study is the same as [28, 45]. Fig. 2 shows the main feature of the trimaran model used in this study, where B/L=0.08, D/L=0.04, C_b=0.52, B_1/L_1=0.05, D_1/L_1=0.04, C_{b1}=0.46, p_L/L=0, p_T/L=0.1, and L, B, D, are the waterline length, waterline width, and draft of the center hull, respectively. L_1, B_1, D_1 are the parameters of the side hull. kxx=2, kyy=25, kzz=27, KG=0.7, LCG=1.0, where (kxx, kyy, kzz) are the moment of inertia; the unit is $kg \cdot m^2$. KG is the Keel to Gantry; the unit is m. LCG is the longitudinal centre of gravity; the unit is m.

The point of nozzle force was located at the centre of the ship's stern. The trimaran model was used for numerical simulation, and the computed values were compared with the results in [3]. The turning manoeuvre in calm water was simulated first. When the simulation started, the trimaran moved forward at a constant speed, and the ship-length Froude number Fn=0.35 was used as the initial trimaran speed for numerical simulation. The nozzle angle was set to δ=25°.

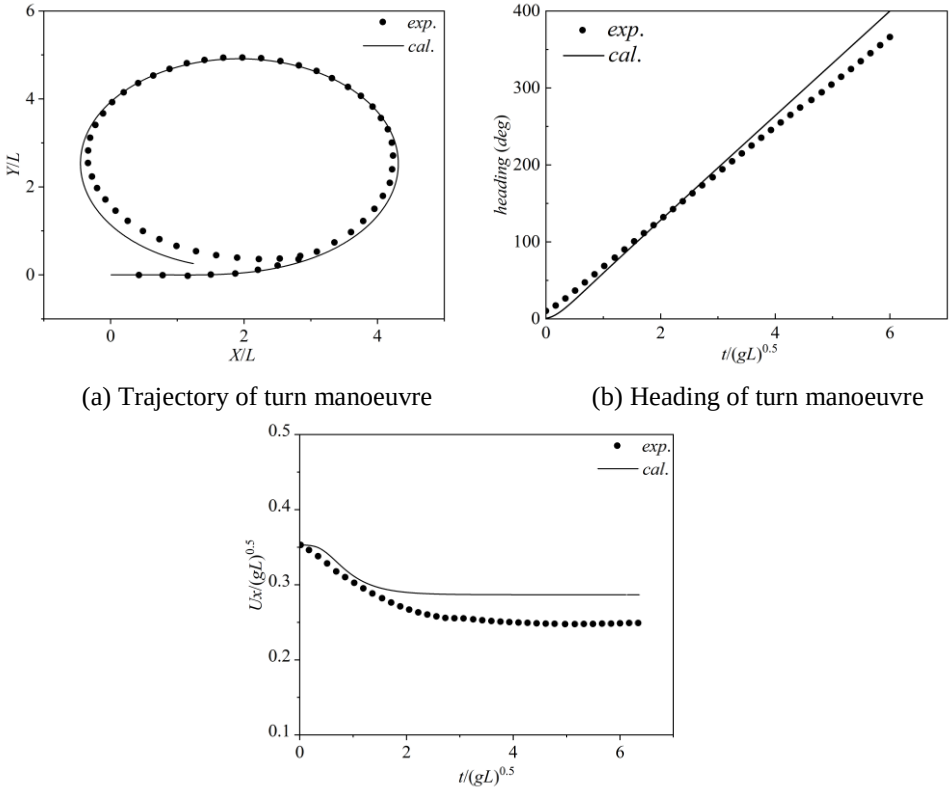

(a) Trajectory of turn manoeuvre (b) Heading of turn manoeuvre

(c) the velocity of the turn manoeuvre

Fig. 3 Computed results of turn manoeuvre in calm water

Fig. 3 shows the computed results of the turn manoeuvre in calm water. The simulation shows that the turning circle simulated by the MMG method based on hydrodynamic derivatives was in good agreement with the simulation results in terms of the manoeuvring trajectory and heading angle, as shown in Fig. 3 (a) and (b). The results proved the correctness and feasibility of the manoeuvrability module calculation program. Fig. 3 (c) shows that the velocity error was approximately 10%, probably because the effect of the hull attitude was not considered, and the propulsion and steering of the waterjet impetus were replaced by the empirical method. The turning circle manoeuvre of the trimaran model in waves was predicted in this section, and the simulation was performed with λ/L=0.88, ak=0.058, β_0=180°, Fn=0.35, where λ is the wavelength, ak is the wave steepness, V_0 is the initial ship speed, Fn is the ship-length Froude number, and β_0 represents the initial wave heading.

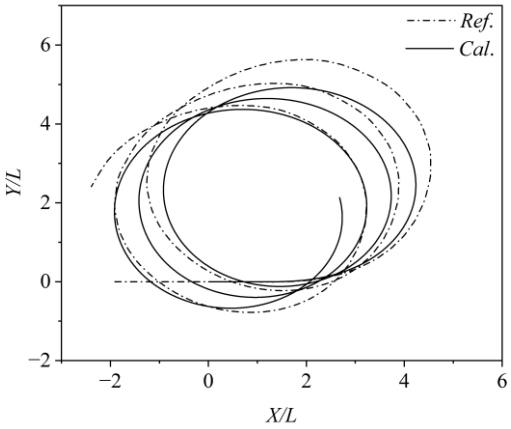

(a) Trajectory of turn manoeuvre

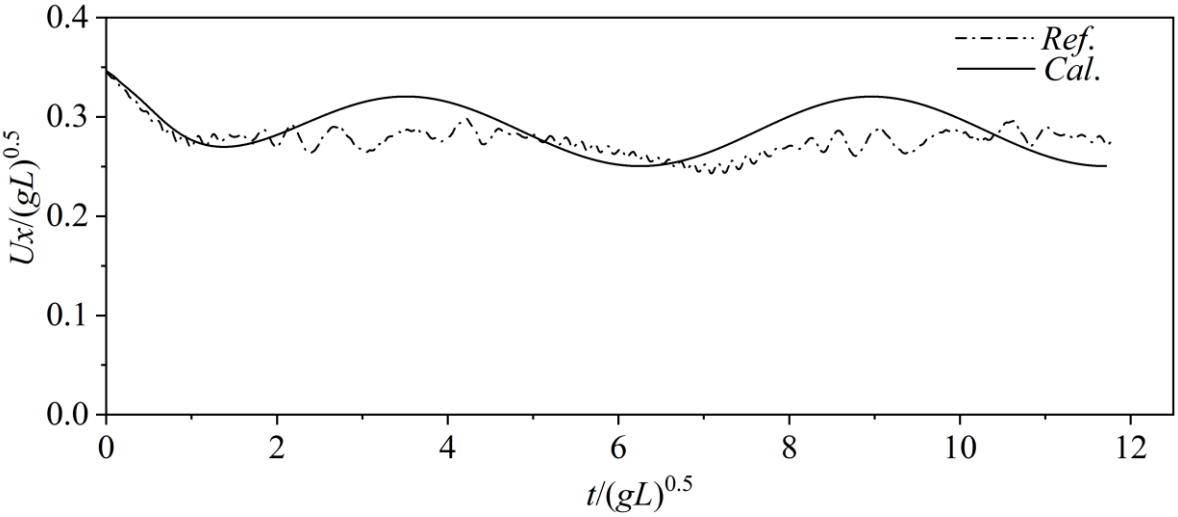

(b) Velocity during the turn manoeuvre

Fig. 4 Computed results of turn manoeuvre in the wave

Fig. 4 shows that because this study applied the second-order average wave-drifting force, the effect of the waves on the ship trajectory drift was considered, and the drift of the turning trajectory led by the waves could be obtained. However, the average wave-drifting force variation was mainly due to the wave heading change, and the effect of the wave phase variation was neglected, so no high-frequency velocity oscillation could be observed using the MMG method. Due to the complexity of the physical problem, the accuracy of the MMG method was enough for the pre-study of the PID parameters' effect on the course-keeping of the trimaran in waves. Similar discrepancies were also observed in [46-47]. The wave heading significantly impacts ship stability when sailing in stern waves [12]. The stern and oblique stern waves posed the greatest threat to the ship's navigation safety due to their tendency to deflect and challenging controllability [28]. Therefore, the working conditions of different initial wave directions were simulated to study the influence of wave direction on the trimaran sailing with waves.

4 Results and Discussions

This section predicts the course-keeping of the trimaran in waves using the MMG method to test the effect of the PID parameter quickly. Then, the trimaran autopilot with the optimized PID parameters was simulated using the hybrid method.

4.1 Course-keeping with Different PID Parameters Using the MMG Method

This section discusses the trimaran's course-changing and course-keeping simulation with different ω_n and the corresponding PID parameters. The initial heading of the trimaran was marked as 0°, and the target heading angle was -20°. The effects of control parameters on the heading angle and motion are discussed. Compared to the 6DOF autopilot simulation, the MMG method proved to be more efficient and suitable for predicting the navigation of the trimaran in waves with many PID parameters. Therefore, taking advantage of the MMG method's high efficiency, the PID parameters' effects on the course changing and course-keeping of the trimaran are examined.

Table 3 The working condition of numerical simulation of manoeuvre in waves

Case	ω_n	λ/L	ak	β_0 (°)	Fn
1	0.084	0.88	0.058	10 30	0.35
2	0.094				
3	0.104				
4	0.114				
5	0.124				
6	0.134				
7	0.144				
8	0.154				

Table 3 shows the working conditions, where λ is the wavelength, a is the wave amplitude, k is the wave number, ak represents the wave steepness, and β_0 is the initial wave heading. The Fn=0.35 was selected as the initial forwarding speed, which corresponded to the design speed of the trimaran. Two initial wave headings, 10° and 30°, of the oblique stern waves were used as the initial wave directions. As [7] suggested, the value of ω_n is around 0.1 for the smaller ship, so ω_n varied from 0.084 to 0.154. When ω_n exceeded the range, the navigation process was no longer stable and led to significant deviations, as shown in Fig. 5.

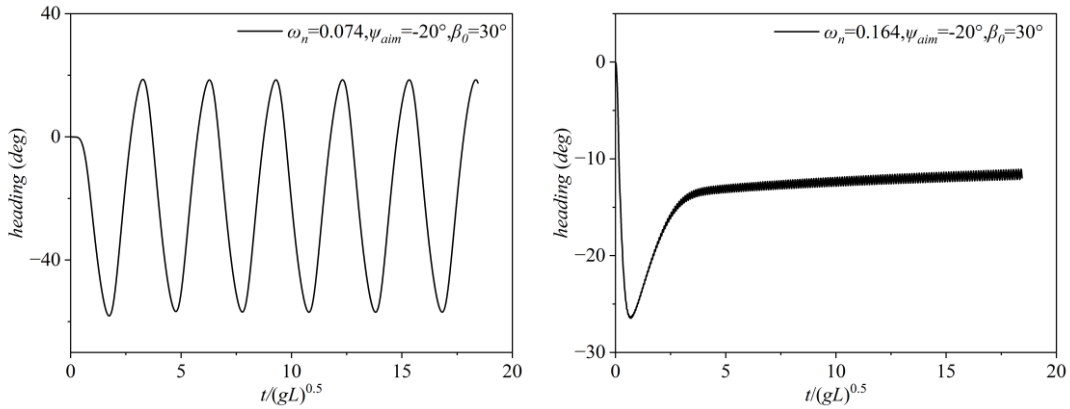

(a) heading angle of ω_n=0.074 (b) heading angle of ω_n=0.164

Fig. 5 Heading of the trimaran with ω_n out of the scope

Fig. 5 shows the heading of the trimaran with the PID parameters corresponding to the ω_n out of the suggested range. The working condition was λ/L=0.88, ak=0.058, β_0=30°, ψ_{aim}=-20°. The case ran for 100s. The peak value of the amplitude appeared when ω_n was about 0.084. If ω_n was smaller because the water jet propulsion was not enough to completely balance the wave force, and the course of the ship produced a large overshoot. Instability occurred in the vicinity of the target heading angle, and its accuracy decreased, especially the

response speed degraded, and the system dynamic characteristics deteriorated, as shown in Fig. 5(a). If ω_n was greater than 0.154, as shown in Fig. 5(b), it caused excessive overshoot in the course control process, prolonged the adjustment time, and even made it difficult to eliminate the static error. Therefore, the range of ω_n was originally determined between (0.084 - 0.154).

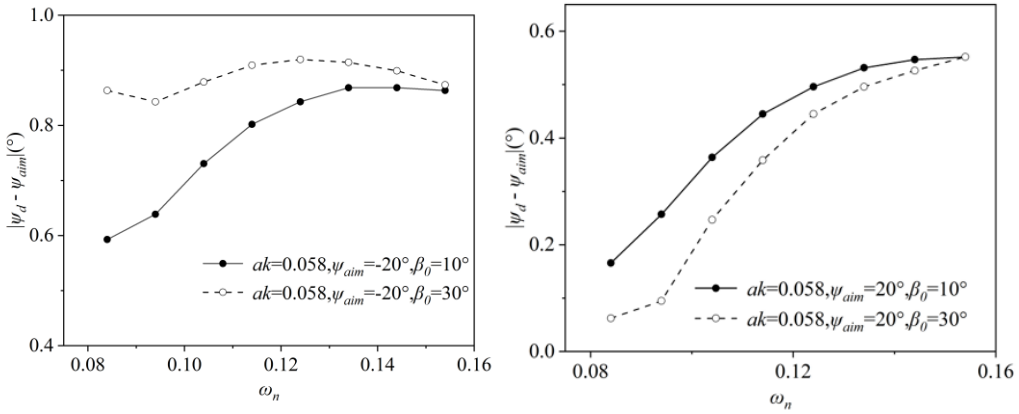

(a) Target heading angle $\psi_{aim} = -20\,°$ (b) Target heading angle $\psi_{aim} = 20°$

Fig. 6 Computed results of PID course-keeping

Fig. 6 shows that regardless of whether the initial wave direction was 10° or 30°, the course deviation variation trend corresponding to different ω_n was the same. Compared with the wave heading control in Fig. 6(a), the stern oblique waves control in Fig. 6(b) is more difficult to control, and the minimum course deviation increases from around 0.2 to 0.6. A comparison of the different initial wave direction results shows that the encountered wave direction changed the course control accuracy, as shown in Fig. 6 (b), when ω_n increases from 0.084 to 0.154. The heading deviation increases gradually. Increasing the control parameters ω_n caused an overshoot.

Since the mean second-order wave force simulation adopted by the MMG method cannot reflect the waves' real-time changes, this study used MMG for pre-study and CFD for further simulation research after reducing the number of examples. According to the size of the deviation, this study selected ω_n=0.084, 0.094, 0.104 working conditions for further CFD calculation. Table 4 shows the PID control parameters to ω_n during simulation.

Table 4 The PID control parameters for different ω_n

ω_n	ζ	T, K	K_p	K_d	K_i
0.084	1.0	6.389, 0.0284	1.5875	2.583	1.08E-05
0.094	1.0	6.389, 0.0284	1.988	7.0827	1.51E-05
0.104	1.0	6.389, 0.0284	2.4335	11.5825	2.04E-05
0.114	1.0	6.389, 0.0284	2.9239	16.0823	2.69E-05
0.124	1.0	6.389, 0.0284	3.4594	20.582	3.46E-05
0.134	1.0	6.389, 0.0284	4.0399	25.0818	4.37E-05
0.144	1.0	6.389, 0.0284	4.6654	29.5815	5.42E-05
0.154	1.0	6.389, 0.0284	5.3358	34.0813	6.63E-05

4.2 The Simulation of the Autopilot in Waves

This section further examines the control parameters of CFD self-propulsion simulations obtained using the MMG method in the previous section.

According to the MMG method results, it is difficult to control the course when the target course angle is -20° and the initial wave direction is 30°. Therefore, this paper focuses on the ship heading control under this working condition through 6DOF self-propulsion simulation. This section further investigates the corresponding optimal control parameters under different conditions using the hybrid CFD solver QaleFOAM, including wavelength λ/L, steepness ak, and speed Fn. All of the ship's 6DOF autopilot simulations was based on the open-source CFD toolbox, OpenFOAM, and the self-developed solver, QaleFoam [48]. The trimaran moved in the oblique wave, and the initial wave heading was β=30°. The case ran for the 30s.

Table 5 shows the details of the working conditions. Since the resonance point of the ship was around λ/L=1.1, a wavelength of 1.09 was selected. The drift force was larger at small wavelengths, so λ/L=0.88 was chosen [45]. A commonly used linear wave $ak = 0.058$ and a large steep nonlinear wave ak=0.135 were selected. Grid and time step convergence studies were carried out using the grid convergence index (GCI) method in our previous work [49]. Figs. 7(a) and (b) illustrate the grid near the free surface and the hull surface, respectively. Because the ship was on autopilot in waves, and the wave heading to the ship varied with every time step, the grid was refined to both the longitudinal and transverse direction in the wave propagation region.

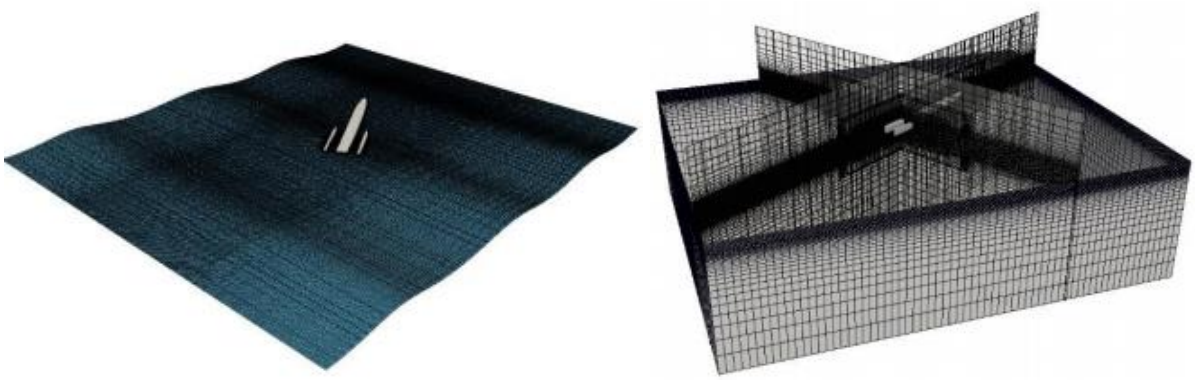

Fig. 7 Sketch of the mesh of domain and hull surface

Table 5 Working conditions for the simulation of trimaran moving in waves at various ω_n

Fn	ak	λ/L	ω_n	β_0
0.35	0.058	0.88	0.084,0.094,0.104	-20°
0.35	0.058	1.09	0.084,0.094,0.104	-20°
0.50	0.135	1.09	0.084,0.094,0.104	-20°
0.60	0.135	1.09	0.084,0.094,0.104	-20°

Fig. 8 compares the heading deviation for different ω_n in four cases. Fig. 8(a) shows that for a small wavelength λ/L=0.88 and steepness ak=0.058, only a minor control force was required to maintain the heading because the wave drift force was small. Conversely, larger control parameters increased the heading overshoot. Fig. 8(a) and (b) show that different control parameters have obvious differences from the beginning for wavelet steepness. Moreover, Fig. 8 shows that the first peak value of heading deviation corresponds to different ω_n and almost coincides because the PID controller had to reach the maximum first wave peak at the beginning. This form control parameter result was closer to the optimal control. This also justifies the three control parameters chosen by the 3DOF MMG method.

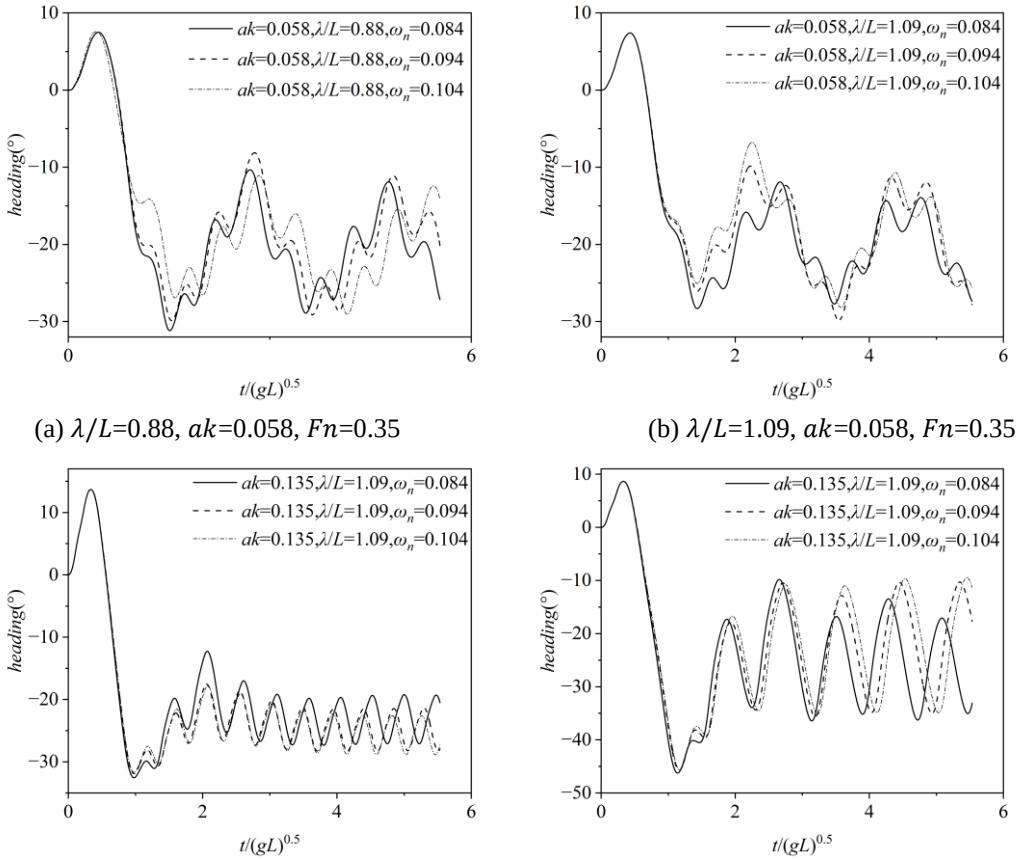

(a) λ/L=0.88, ak=0.058, Fn=0.35 (b) λ/L=1.09, ak=0.058, Fn=0.35

(c) λ/L=1. 09, ak=0.135, Fn=0.50 (d) λ/L=1.09, ak=0.135, Fn=0.60

Fig. 8 The effect of ω_n on the course deviation at different wave parameters and forward speeds

Fig. 8(a) and (b) show that when the wavelength increases to λ/L =1.09, the time to reach the peak is about 2s earlier, and the control parameters corresponding to the smallest change in heading angle are also applicable to small wavelengths. Fig. 8(b) and (c) show that the optimal control parameters in small wave steepness produce a large heading overshoot when the wave steepness increases. Due to the increase of wave drift force, the restoring moment needs a longer distance to bring the ship back to the target course and ω_n =0.089 cannot eliminate the corresponding wave force drift, so the course deviation is larger. Combining Fig. 8(b) and Fig. 8(c) show that when the speed Fn=0.35, a larger wave steepness ak=0.135 lead to more frequent nozzle deflection, making it more difficult to control the course of the ship. This conclusion is supported by Yan et al. [50].

A comparison of Fig. 8(c) and (d) show that the course deviation is larger when the speed increases from Fn=0.50 to Fn=0.60, and the maximum course deviation angle increases by about 30%. Wave steepness has a more pronounced effect on control than wavelength. When the speed increases to Fn=0.60, as shown in Fig. 8 (d), the heading angle changes more noticeably. When the trimaran sailed in the stern oblique wave with a high initial speed, the fast-sailing speed of the trimaran combined with the larger wave steepness may result in a wider yaw range. Consequently, more frequent nozzle adjustment was required.

Note that different cases denoted by (a) and (b) correspond to different wavelengths. Additionally, (b) and (c) represent varying wave steepness, while (c) and (d) depict different Fn values. More importantly, note that the absolute velocity is relatively unaffected by the variations in control parameters. ω_n changes the corresponding nozzle rotation angle through the PID controller, and the corresponding propulsion force component changes accordingly. ω_n changes the corresponding nozzle rotation angle through the PID controller and adjusts the

propulsion force component accordingly. Since the control parameters solely act on the rotation angle of the nozzle to maintain the heading, different control parameters correspond to diverse control times, resulting in a certain time gap required to reach the maximum speed.

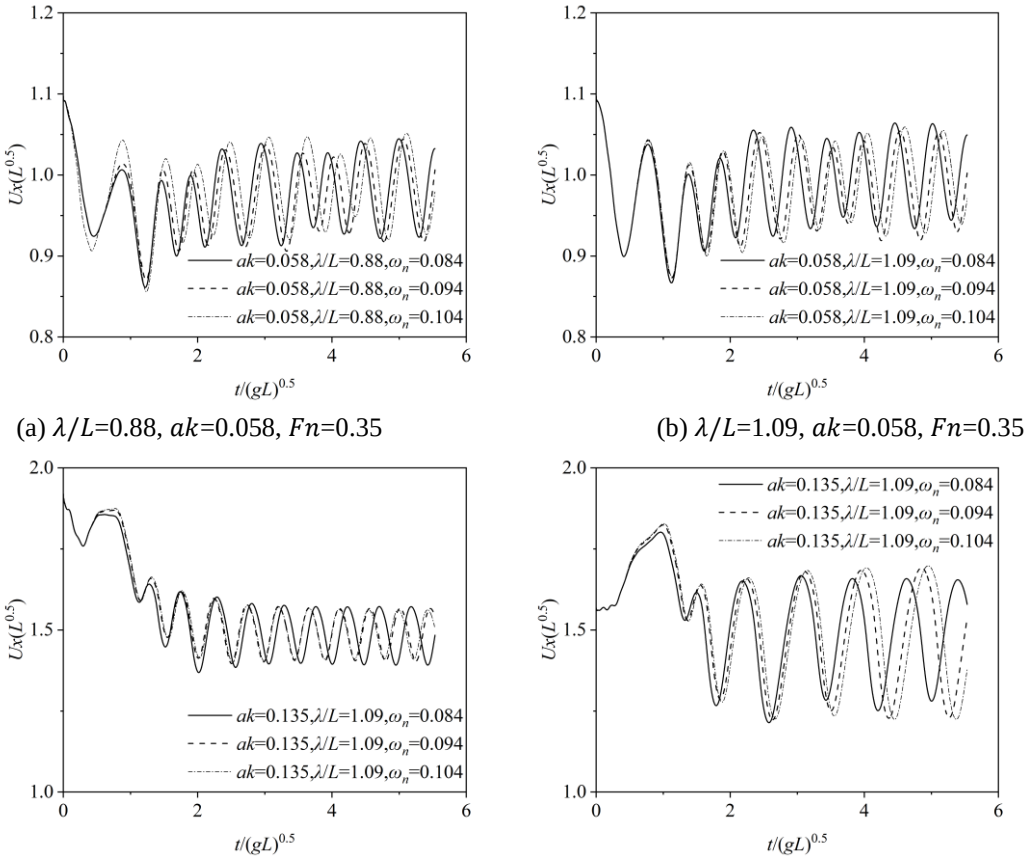

(a) λ/L=0.88, ak=0.058, Fn=0.35

(b) λ/L=1.09, ak=0.058, Fn=0.35

(c) λ/L=1.09, ak=0.135, Fn=0.50

(d) λ/L=1.09, ak=0.135, Fn=0.60

Fig. 9 The effect of ω_n on the Ux at different wave parameters and forward speeds

This phase difference is amplified at ak = 0.135. Fig. 9 and Fig. 10 show that different control parameters correspond to different heave phases. One possible reason for this phenomenon is that different ω_n values correspond to different forward speeds, thereby causing the ship to experience various wave phases, resulting in diverse heave phases. Fig. 10(b) shows that when the wavelength increases from λ/L = 0.88 to λ/L = 1.09, the amplitude of the heave motion with the same control parameters increases by about 15%. Additionally, Fig. 10(c) and (d), show that when the speed increases to Fn=0.60, the velocity and heave motion exhibit more obvious nonlinearity. The periodic fluctuations can be observed in Fig. 10(a), (b), and (c), but not in Fig. 10(d). The trimaran's speed was still fluctuating because it was not caught by the stern oblique wave. As the wave speed exceeded the trimaran's speed, the stern oblique waves periodically impacted the ship. Observe that for the wavelength λ/L =1.09, the wave steepness has a significant effect on the heave of the oblique wave. The increase in wave steepness resulted in a more pronounced heave motion, as shown in Fig. 10 (c) and (d). The steady heave values are almost the same for different speeds.

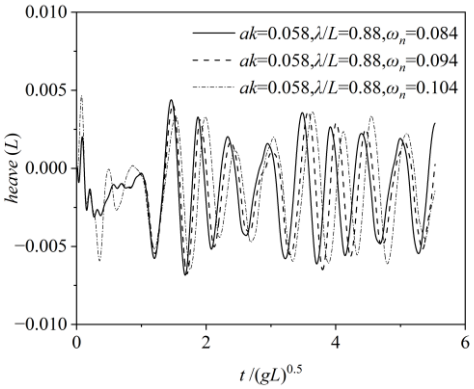

(a) λ/L=0.88, ak=0.058, Fn=0.35

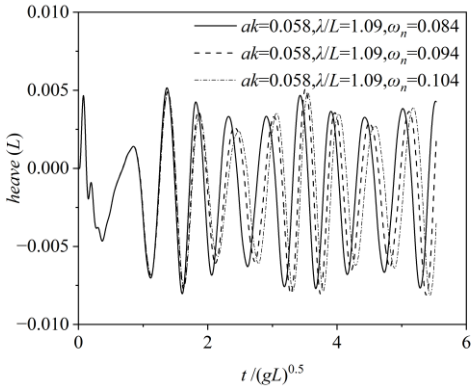

(b) λ/L=1.09, ak=0.058, Fn=0.35

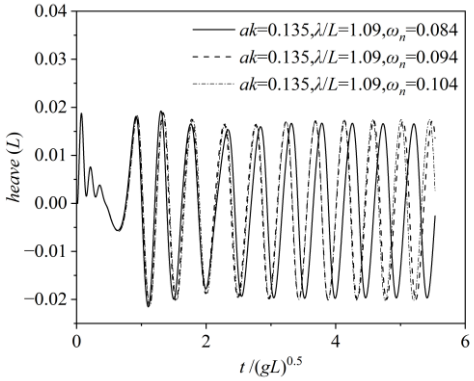

(c) λ/L=1.09, ak=0.135, Fn=0.50

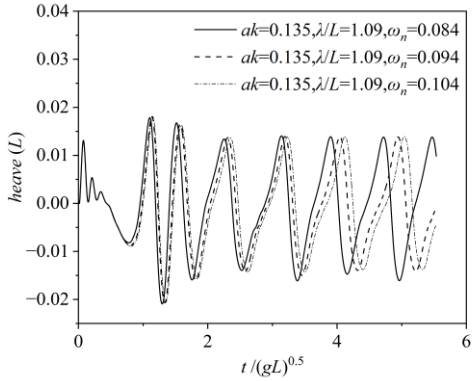

(d) λ/L=1.09, ak=0.135, Fn=0.60

Fig. 10 The effect of ω_n on the heave at different wave parameters and forward speeds

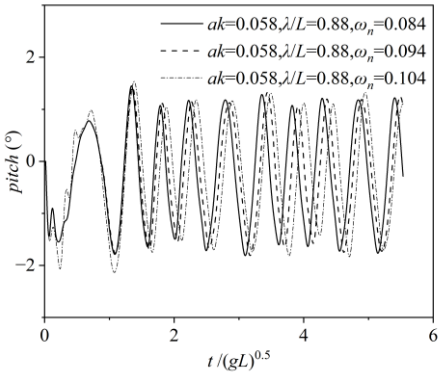

(a) λ/L=0.88, ak=0.058, Fn=0.35

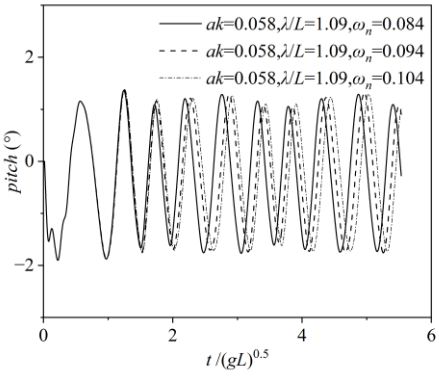

(b) λ/L=1.09, ak=0.058, Fn=0.35

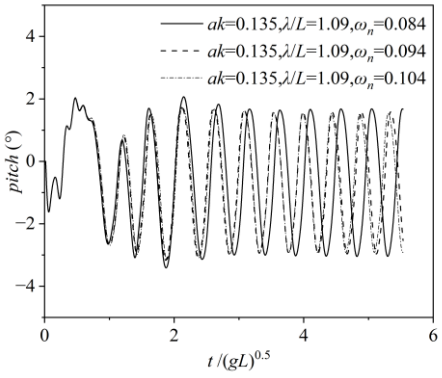

(c) λ/L=1.09, ak=0.135, Fn=0.50

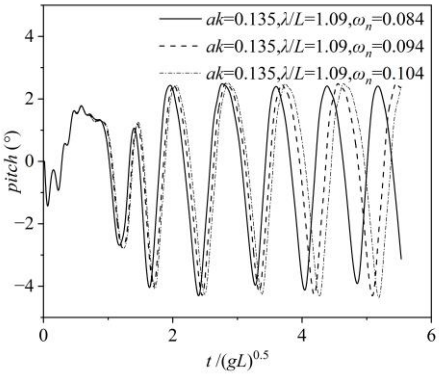

(d) λ/L=1.09, ak=0.135, Fn=0.60

Fig. 11 The effect of ω_n on the pitch at different wave parameters and forward speeds

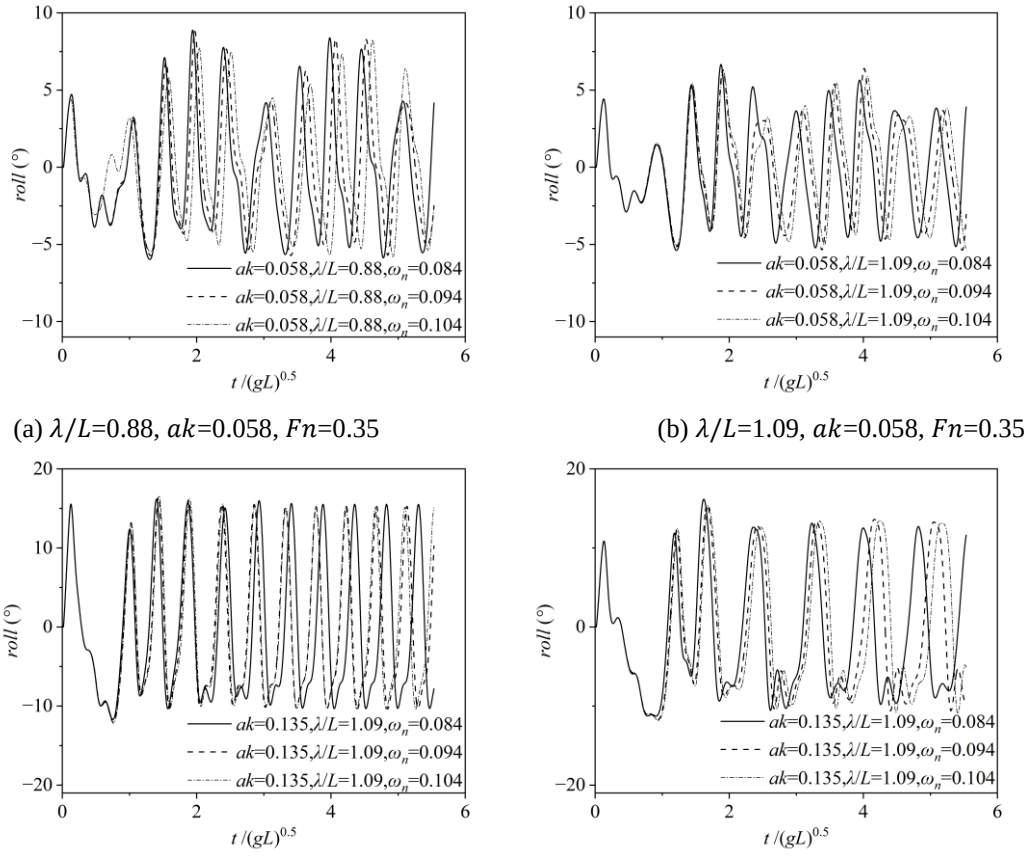

(a) λ/L=0.88, ak=0.058, Fn=0.35

(b) λ/L=1.09, ak=0.058, Fn=0.35

(c) λ/L=1.09, ak=0.135, Fn=0.50

(d) λ/L=1.09, ak=0.135, Fn=0.60

Fig. 12 The effect of ω_n on the roll at different wave parameters and forward speeds

Fig. 11 and Fig. 12 show the trimaran's pitch and roll motions in oblique stern waves. Comparing the effects of wavelength and wave steepness shows that the effect of wavelength on motion amplitude is smaller than wave steepness, possibly because the greater the wave steepness, the more frequent the nonlinear phenomenon, resulting in greater shaking. Comparing the results at different wavelengths, as shown in Fig. 11(a) and (b), observe that the wavelength has little effect on the pitching motion tendency. Different control parameters have little effect on low-speed heave and roll motions. Fig. 11(b) and (c) compare the same wave steepness at different wavelengths, indicating that the pitching motion increases markedly with increasing wave steepness. Fig. 11(d) shows that the stable period corresponds to ω_n=0.084 when the ship is in a stable state and is reduced by approximately 10 % compared with ω_n=0.104 because at high speed (Fn=0.60) a tiny control can have a big impact on course-keeping, and only a small control is needed to achieve heading hold.

A comparison of Fig. 12(a) and (b) shows that as the wavelength changes, the optimal control parameters corresponding to roll also change. When the wavelength is small, the roll amplitude corresponding to ω_n=0.084 is the best. However, when the wavelength increases to λ/L =1.09, the roll of ω_n=0.094 is relatively small. Fig. 12(c) and (d) show that when the wavelength = 1.09, the high speed of Fn =0.6 is beneficial to reduce roll.

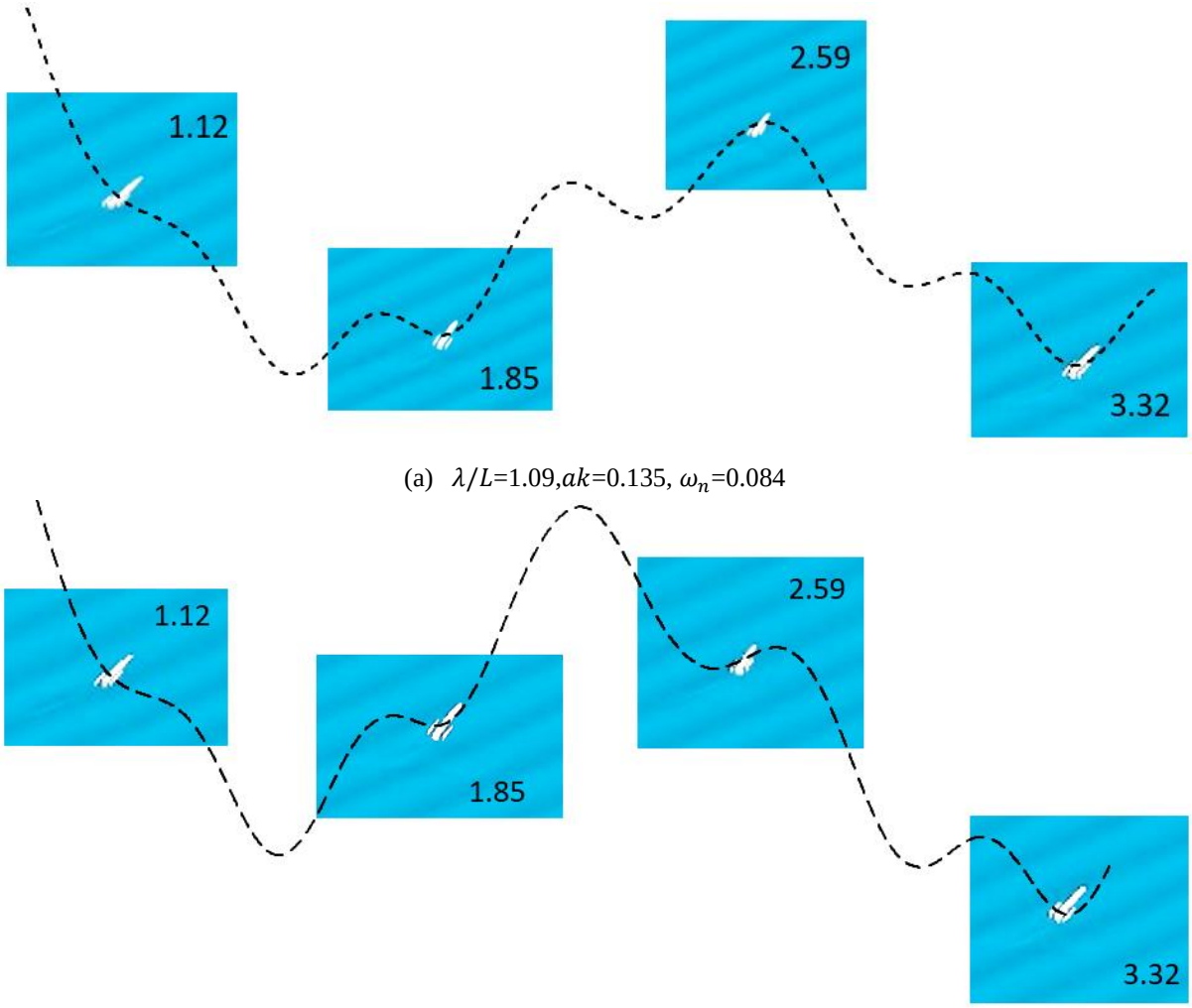

(a) λ/L=1.09,ak=0.135, ω_n=0.084

(b) λ/L=1.09,ak=0.135, ω_n=0.104

Fig. 13 The wave profile during the simulation at various ω_n.

Fig. 13 shows the autopilot trimaran wave profiles in oblique stern waves and the wave profiles at time 1.12, 1.85, 2.59, and 3.32. The dashed line represents the ship's heading. Fig. 13(a) shows that when the wave peak is at the stern side, the larger wave steepness makes the trimaran's left side hull sink deeper into the wave. After the wave peak passes the centre of the trimaran, the wave peak helps to slow down the deflection of the heading. Fig. 13(a) and (b) also show that when the control bandwidth ω_n increases, the increase in response speed of the heading angle is attributed to the large control parameter. By combining Fig. 13(a) with Fig. 12(d), it is evident that at time 1.12, the ship is situated in a lower wave profile, and the hull is tilted to the left side, resulting in a negative ship roll. However, Figure 13(b) shows that at time 3.32, the ship is situated within the higher wave profile, and the hull is inclined towards the right side, resulting in a positive roll for the trimaran. Therefore, the simulated ship motion aligns with the practical situation.

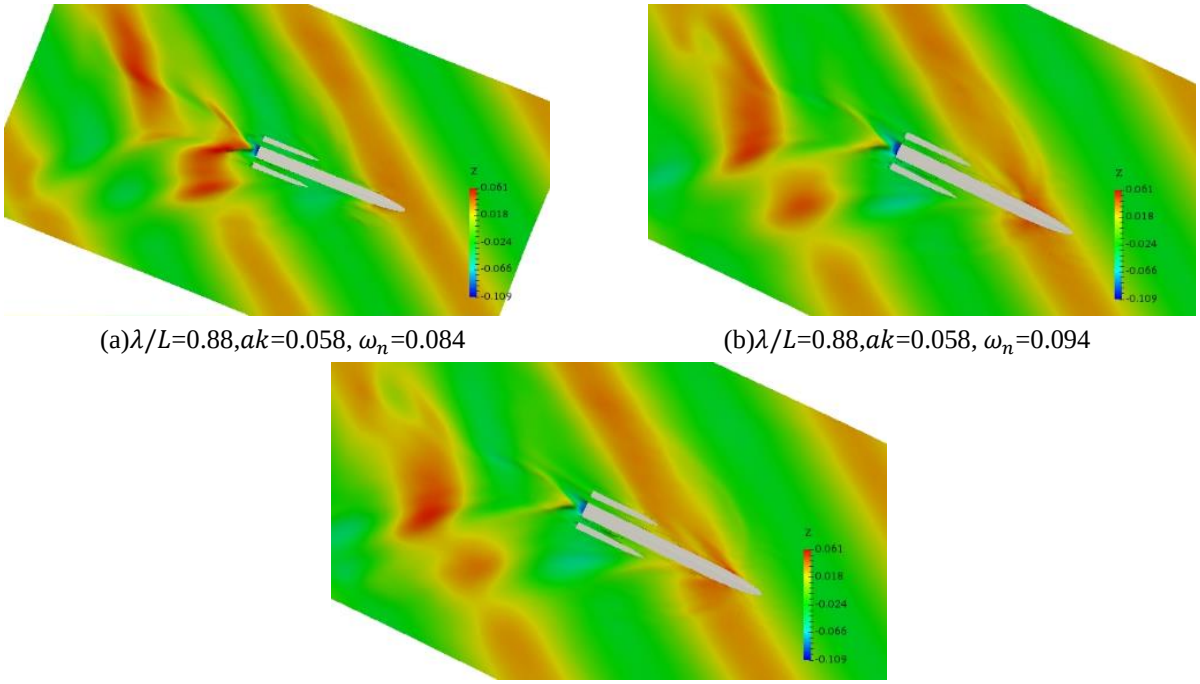

(a)λ/L=0.88,ak=0.058, ω_n=0.084 (b)λ/L=0.88,ak=0.058, ω_n=0.094

(c) λ/L=0.88,ak=0.058,ω_n=0.104

Fig. 14 Wave profile during the autopilot in oblique stern waves at Fn=0.35

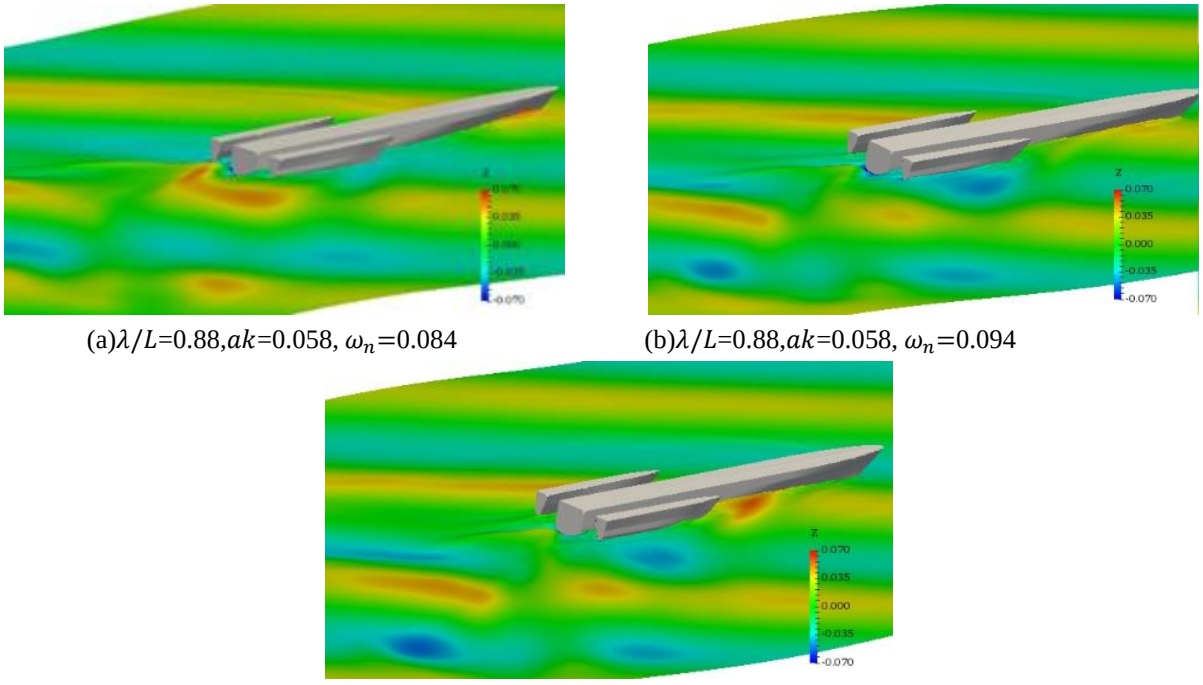

(a)λ/L=0.88,ak=0.058, ω_n=0.084 (b)λ/L=0.88,ak=0.058, ω_n=0.094

(c) λ/L=0.88,ak=0.058,ω_n=0.104

Fig. 15 Wave profile during the autopilot in oblique stern waves at Fn =0.50

Fig. 14 and Fig. 15 show the wave ship's profile on the stern oblique waves is, which are captured when the difference between the ship headings by different PID parameters is most significant. Two working conditions were selected, and the results of the three PID parameters were compared under each working condition. Fig. 14 shows the yaw forces and moments generated by waves. Under the influence of oblique stern waves, the wave elevation on the ship's portside is more significant than the starboard. The wave heights of the wave profiles in

Fig. 14(a) and (b) are different, possibly due to the reduction of certain control parameters and the advancement of the nozzle rotation time.

The turning of the nozzle timing has a limited influence on direction. Fig. 15(c) shows that the larger natural frequency at low speeds gives the trimaran a greater rolling. Fig. 12(a), (b), and (c) support this conclusion. Fig. 15 shows no significant difference in the wave phase with the largest title deviation, and the larger control parameters correspond to larger deflection angles. Fig. 9(c) and (d) show that the range of speed change is significantly larger when Fn=0.6 compared to Fn=0.5. Fig. 14 and Fig. 15 show that at the maximum yaw, the coupling of pitch and roll motion at high-speed Fn=0.6 is not obvious compared with low speeds.

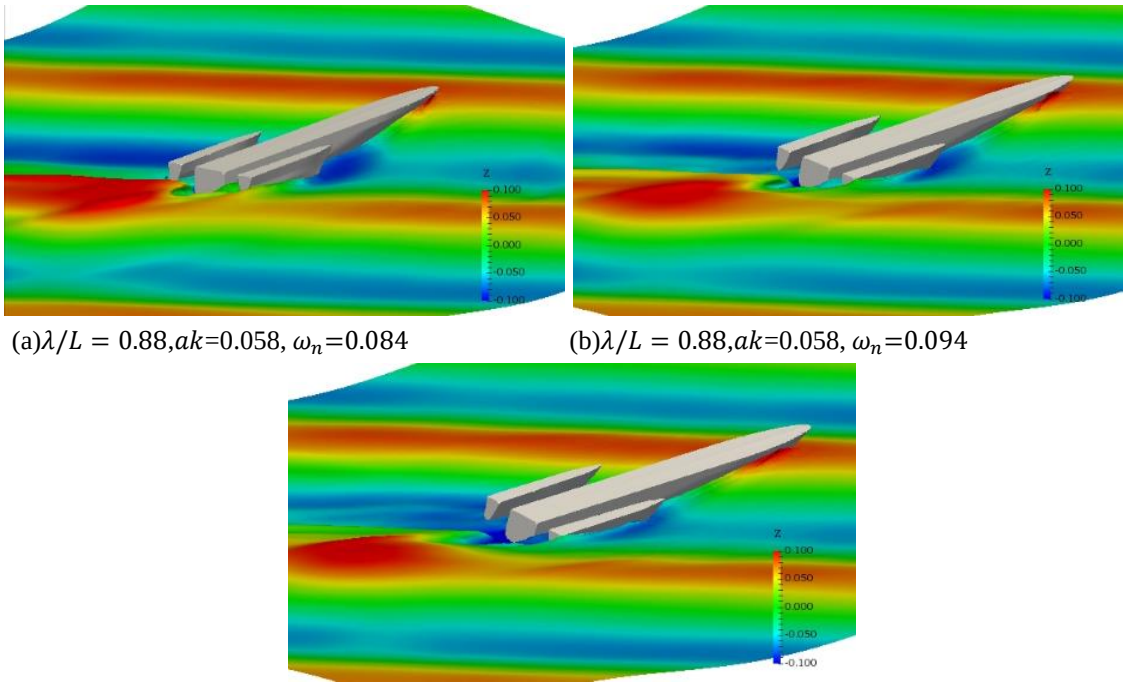

(a)λ/L = 0.88,ak=0.058, ω_n=0.084 (b)λ/L = 0.88,ak=0.058, ω_n=0.094

(c)λ/L = 0.88,ak=0.058,ω_n=0.104

Fig. 16 Wave profile during the autopilot in oblique stern waves at Fn =0.60

Fig. 16 shows that the trimaran is difficult to control under the oblique stern wave and is easily captured by waves due to high speed. Fig. 16(a) and (c) compare the trimaran in diverse ω_n conditions. When ω_n = 0.104, the nonlinear phenomenon, such as green water and pitch motion, is more obvious. A comparison of Fig. 15 and Fig. 16 indicates that under the same wave, waves are more likely to capture higher speeds, resulting in surf-riding.

Conclusion

This study conducted numerical simulations using the 3DOF MMG and 6DOF self-propulsion simulation methods based on CFD to simulate the manoeuvrability of a trimaran. It focuses on the effects of different control parameters on the ship's course control in oblique stern waves. Several conclusions can be drawn by analysing the calculation results.

The PID controller parameters based on hydrodynamic derivatives are suitable for simulating the motion of the trimaran in oblique stern waves. Though the simulation of the turning manoeuvre trajectory by the second-order average wave drift force is accurate enough, predicting the speed loss during the turn manoeuvre still needs improvement. Additionally, it is more difficult for a trimaran to maintain its course in stern oblique waves than in stern waves. The specific value of the natural frequency is determined by working conditions. Moreover, it

is more difficult for a trimaran to maintain its course in stern oblique waves than in oblique waves. In the case of initial wave direction of 20° and -20°, the course control effect of ω_n = 0.084 is better only when the wavelength λ/L=1.09, wave steepness ak=0.135, and the heading angle control effect ω_n=0.094.

The nozzle angle phase can be altered by changing the natural frequency under the same working conditions, leading to different peak velocities while the absolute speed remains unchanged. When the trimaran muzzle velocity is Fn =0.60, both velocity and heave motion show significant nonlinearity. The wave steepness notably affects the heave motion, with higher wave steepness resulting in a more pronounced heave motion. In particular, large and steep waves (ak=0.135) make the influence of different control parameters on the heave phase more noticeable.

The small control variable has a significant impact on the course at high speed (Fn=0.60), requiring only small adjustments to the control variable to maintain the desired direction. Under the same conditions, higher speeds are beneficial for reducing roll when the wavelength (λ/L=1.09). However, a larger natural frequency results in greater trimaran rolling at low speeds.

This study conducted simulations of various natural frequencies of a trimaran's PID controller. However, the control corresponding to different initial wave directions may also have a significant impact, requiring further study.

Acknowledgement

This project was supported by the National Natural Science Foundation of China (Grant number 51979157), and the Science and Technology Commission of Shanghai Municipality, China (Grant number 22YF1415900).

Reference

[1] Seo, M. G., Kim, Y., 2021. Numerical analysis on ship maneuvering coupled with ship motion in waves. *Ocean Engineering*, 38(17-18), 1934-1945. https://doi.org/10.1016/j.oceaneng.2011.09.023

[2] Wang, J., Wan, D., 2018. CFD investigations of ship maneuvering in waves using naoe-FOAM-SJTU Solver. *Journal of Marine Science and Application*, 17(3), 443-458. https://doi.org/10.1007/s11804-018-0042-4

[3] Gong, J., Li, Y., Jiang, F., Hong, Z., Yu, D., 2020. Maneuvering simulation and study on the effect of hull attitude on maneuverability of trimarans by OpenFOAM. *Journal of Coastal Research*, 36(1), 157-173. https://doi.org/10.2112/JCOASTRES-D-19-00086.1

[4] Nicholson, K. 1974. Some parametric model experiments to investigate broaching-to. In International Symposium on the Dynamics of Marine Vehicles and Structures in Waves, London.

[5] Jong, P.D., Renilson, M.R., Walree, F.V., 2013. The broaching of a fast rescue craft in following seas. In: *Proceedings of the 12th International Conference on Fast Sea Transportation*, 2-5 December, Amsterdam, Netherlands.

[6] IMO, 2019. Finalization of second generation intact stability criteria. In: Report of the Experts' Group on Intact Stability, SDC 6/WP.6, London, UK.

[7] Fossen, T.I., 2011. Handbook of marine craft hydrodynamics and motion control. John Wiley & Sons, Hoboken, New Jersey, USA. https://doi.org/10.1002/9781119994138

[8] Maki, A., Sakamoto, N., Akimoto, Y., Banno, Y., Maniyappan, S., Umeda, N., 2021. On broaching-to prevention using optimal control theory with evolution strategy. *Journal of Marine Science and Technology*, 26(1), 71-87. https://doi.org/10.1007/s00773-020-00722-9

[9] Minorsky, N., 1922. Directional stability of automatically steered bodies. Journal of the American Society for Naval Engineers, 34(2), 280-309. https://doi.org/10.1111/j.1559-3584.1922.tb04958.x

[10] Van Amerongen, J., 1984. Adaptive steering of ships-A model reference approach. *Automatica*, 20(1), 3-14. https://doi.org/10.1016/0005-1098(84)90060-8

[11] Im, N., and Seo, J. H., 2010. Ship manoeuvring performance experiments using a free running model ship. *TransNav, International Journal on Marine Navigation and Safety od Sea Transportation*, 4(1).

[12] Hashimoto, H., Umeda, N., and Matsuda, A., 2011. Broaching prediction of a wave-piercing tumblehome vessel with twin screws and twin rudders. *Journal of marine science and technology*, 16(4), 448-461. https://doi.org/10.1007/s00773-011-0134-1

[13] Ghareaghaji, A., 2015. A comparison between Fuzzy-PSO controller and PID-PSO controller for controlling a DC motor. *Bulletin of Electrical Engineering and Informatics*, 4(2), 130-135. https://doi.org/10.11591/eei.v4i2.328

[14] Umeda, N., Usada, S., Mizumoto, K., and Matsuda, A., 2016. Broaching probability for a ship in irregular stern-quartering waves: theoretical prediction and experimental validation. *Journal of Marine Science and Technology*, 21(1), 23-37. https://doi.org/10.1007/s00773-015-0364-8

[15] Sadat-Hosseini, H., Araki, M., Umeda, N., Sano, M., Yeo, D. J., Toda, Y., Stern, F., 2011. CFD, System-Based Method, and EFD Investigation of ONR Tumblehome Instability and Capsize with Evaluation of the Mathematical Model. *12th International Ship Stability Workshop*, 12-15 June, Washington DC.

[16] Hashimoto, H., Stern, F., Hosseini, S. H. S., 2008. 2008S-G2-6 An Application of CFD for Advanced Broaching Prediction (2nd Report). *Conference Proceedings The Japan Society of Naval Architects and Ocean Engineers*, 6, 237-240.

[17] Hashimoto, H., Stern, F., Sadat Hosseini, S. H., Sueyoshi, M., 2008. An Application of CFD to Recent Ship Stability Problems. *10th International Ship Stability Workshop*, 23-25 March 2008, Daejeon, South Korea.

[18] Wang, L., 2020. PID control system design and automatic tuning using MATLAB/Simulink. John Wiley & Sons. https://doi.org/10.1002/9781119469414

[19] Dubey, A. C., Gajapathy, R., Rajendran, S., 2021. An experimental and numerical investigation on the autopilot design of a KVLCC2 tanker. In OCEANS 2021: San Diego–Porto, 20-23 September, IEEE, 1-6. https://doi.org/10.23919/OCEANS44145.2021.9705853

[20] Nataraj, C., Bolla, S., Samanta, B., 2015 Analysis & Design Of An Adaptive Autopilot: Theory & Experiments.

[21] Maniyappan, S., Umeda, N., Maki, A., Akimoto, Y., 2021. Effectiveness and mechanism of broaching-to prevention using global optimal control with evolution strategy (CMAES). *Journal of Marine Science and Technology*, 26(2), 382-394. https://doi.org/10.1007/s00773-020-00743-4

[22] Castiglione, T., Sadat-Hosseini, H., Stern, F., Bova, S., 2013. CFD Simulation for Course Keeping of Free Running Delft Catamaran in Regular Head and Oblique Waves. *Proceedings of the 12th International Conference on Fast Sea Transportation*, 2-5 December 2013, Amsterdam, Netherlands.

[23] Carrica, P. M., Sadat-Hosseini, H., Stern, F., 2012. CFD Analysis of Broaching for a Model Surface Combatant with Explicit Simulation of Moving Rudders and Rotating Propellers. *Computers and Fluids*, 53, 117-132. https://doi.org/10.1016/j.compfluid.2011.10.002

[24] Yasukawa, H., Yoshimura, Y., 2015. Introduction of MMG standard method for ship maneuvering predictions. *Journal of Marine Science and Technology*, 20(1), 37-52. https://doi.org/10.1007/s00773-014-0293-y

[25] Yasukawa, H., Sakuno, R., 2020. Application of the MMG method for the prediction of steady sailing condition and course stability of a ship under external disturbances. *Journal of Marine Science and Technology*, 25(1), 196-220. https://doi.org/10.1007/s00773-019-00641-4

[26] Sadat-Hosseini, H.; Kim, D.; Toxopeus, S.; Diez, M., 2015. CFD and potential flow simulations of fully appended free running 5415 m in irregular waves. *In Proceedings of the 5th World Maritime Technology Conference (WMTC15)*, 3-7 November, Providence, USA. https://doi.org/10.5957/WMTC-2015-152

[27] Kim, D., Song, S., Tezdogan, T., 2021. Free running CFD simulations to investigate ship manoeuvrability in waves. *Ocean Engineering*, 236, 109567. https://doi.org/10.1016/j.oceaneng.2021.109567

[28] Gong, J. Y., Li, Y., Fu, Z., Li, R., Hong, Z. 2022. Study on the characteristics of Trimaran's surf-riding in stern waves by a hybrid method. *Ocean Engineering*, 265, 112603. https://doi.org/10.1016/j.oceaneng.2022.112603

[29] Dai, K., Li, Y.B., Gong, J.Y., Fu, Z., Li, A., Zhang, D.P., 2022. Numerical study on propulsive factors in regular head and oblique waves. *Brodogradnja*, 73(1), 37-56. https://doi.org/10.21278/brod73103

[30] Degiuli, N., Farkas, A., Martić, I., Zeman, I., Ruggiero. V., Vasiljevic, V., 2021. Numerical and experimental assessment of the total resistance of yacht. *Brodogradnja*, 72(3), 61-80. https://doi.org/10.21278/brod72305

[31] Jang Y.H., Eom, M.J., Paik, K.J., Kim, S.H., Song, G., 2020. A numerical study on the open water performance of a propeller with sinusoidal pitch motion. *Brodogradnja*, 71(1), 71-83. https://doi.org/10.21278/brod71105

[32] Gong J Y, Yan S Q, Ma Q W, Li, Y., 2021. Numerical simulation of fixed and moving cylinders in focusing wave by a hybrid method. *International Journal of Offshore and Polar Engineering*, 31(1), 102-111. https://doi.org/10.17736/ijope.2021.jc812

[33] Pollalis C, Mourkogiannis D, Boulougouris E. 2021. Numerical simulation of a vessel's manoeuvring performance in regular waves. *Ships and Offshore Structures*, 17(11), 2498-2507. https://doi.org/10.1080/17445302.2021.2005354

[34] Zhang, Q., Zhang, X.-K., Im, N.-K. 2017. Ship nonlinear-feedback course keeping algorithm based on MMG model driven by bipolar sigmoid function for berthing. *International Journal of Naval Architecture and Ocean Engineering*, 9, 525–536. https://doi.org/10.1016/j.ijnaoe.2017.01.004

[35] Daidola, J.C. 1986. A simulation program for vessel's manoeuvring at slow speeds. *Proceedings of Eleventh ship Technology and Research (STAR) symposium*.

[36] English, J.W., Wise D.A. 1975. Hydrodynamics aspects of dynamic positioning. *Transactions of RINA*, 92(3), 53-72.

[37] Xing T, Carrica P, Stern F, 2008. Computational towing tank procedures for single run curves of resistance and propulsion. *Journal of Fluids Engineering*, 130(10), 1135-1150. https://doi.org/10.1115/1.2969649

[38] Yan, S., Wang, J.H., Wang, J.X., Ma, Q.W., Xie, Z.H, 2019. Numerical Simulation of Wave Structure Interaction using QaleFOAM, *Proceedings of the 29th International Offshore and Polar Engineering Conference*, 16-21 June, Honolulu, Hawaii, USA

[39] Yan, S.Q., Ma, Q.W., 2010. QALE-FEM for modelling 3D overturning waves. *International Journal for Numerical Methods in Fluids*, 63(6), 743–768. https://doi.org/10.1002/fld.2100

[40] Sato, Y., Uzawa, K., Miyata, H., 2007. Validation of motion prediction method for Trimaran vessels. *In 9th International Conference on Numerical Ship Hydrodynamics*, 5–8 August, Michigan USA.

[41] Gong, J.Y., Li, Y.B., Cui, M., Fu, Z., Zhang, D.P., 2021. The effect of side-hull position on the seakeeping performance of a trimaran at various headings. *Ocean Engineering*, 239, 109897. https://doi.org/10.1016/j.oceaneng.2021.109897

[42] Rusche, H., 2002. Computational Fluid Dynamics of Dispersed Two-phase Flows at High Phase Fractions. Imperial College, London, UK.

[43] Weller, H.G., 2002. Derivation, Modelling and Solution of the Conditionally Averaged Two-phase Flow Equations. Nabla Ltd. Technical Report TR/HGW/02.

[44] Gong, J., Li, Y., Dai, K., Fu, Z., Hong, Z., 2022. Numerical simulation of ship maneuvring by a hybrid method with propulsive factors in waves taken into account. *Ocean Engineering*, 264, 112538. https://doi.org/10.1016/j.oceaneng.2022.112538

[45] Gong, J., Yan, S., Ma, Q., Li, Y., 2020. Added resistance and seakeeping performance of trimarans in oblique waves. *Ocean Engineering*, 216, 107721. https://doi.org/10.1016/j.oceaneng.2020.107721

[46] Yasukawa H., 2006 Simulations of ship maneuvering in waves: 1st report: turning motion. *Journal of the Japan Society of Naval Architects and Ocean Engineers*, 4, 127–136 (in Japanese). https://doi.org/10.2534/jjasnaoe.4.127

[47] Seo, M., Kim, Y. 2011 Numerical analysis on ship maneuvering coupled with ship motion in waves. *Ocean Engineering*, 38(17–18), 1934–1945. https://doi.org/10.1016/j.oceaneng.2011.09.023

[48] Li, Q., Wang, J. H., Yan, S. Q., Gong, J. Y., Ma, Q. W., 2018. A zonal hybrid approach coupling FNPT with OpenFOAM for modelling wave-structure interactions with action of current. *Ocean Systems Engineering*, 8(4), 381-407.

[49] Li, Y., Li, A., Gong, J., Fu, Z., Dai, K., 2021. Numerical investigation on added resistance and motions of a high-speed trimaran equipped with T-foil and stern flap in regular head and oblique waves for varying wave steepness. *Journal of the Brazilian Society of Mechanical Sciences and Engineering*, 43, 1-21. https://doi.org/10.1007/s40430-021-03177-0

[50] Yan, Z., Zhang, X., Zhu, H., Li, Z., 2020. Course-keeping control for ships with nonlinear feedback and zero-order holder component. *Ocean Engineering*, 209, 107461. https://doi.org/10.1016/j.oceaneng.2020.107461

Submitted: 17.04.2023.
Accepted: 17.10.2023.

Yunbo Li, multihull@163.com
Zongyu Tang,
Jiaye Gong*, gongjiaye@shmtu.edu.cn
College of Ocean Science and Engineering, Shanghai Maritime University, Shanghai 201306, China